ACS Macro Letters

Letter

pubs.acs.org/macroletters

Origin of Stress Overshoot during Startup Shear of Entangled Polymer Melts

Yuyuan Lu,[†] Lijia An,*[,†] Shi-Qing Wang,*[,‡] and Zhen-Gang Wang*[,†,§]

[†]State Key Laboratory of Polymer Physics and Chemistry, Changchun Institute of Applied Chemistry, Chinese Academy of Sciences, Changchun 130022, People's Republic of China

[‡]Department of Polymer Science, University of Akron, Akron, Ohio 44325-3909, United States

[§]Division of Chemistry and Chemical Engineering, California Institute of Technology, Pasadena, California 91125, United States

ABSTRACT: Using Brownian dynamics simulation, we determine the chain orientation and stretching and their connection to stress overshoot in an entangled polymer melt undergoing startup shear at rates lower than the reciprocal of the Rouse time yet higher than the reciprocal of the reptation time. In this rate regime, the prevailing tube theory attributes the stress overshoot to alignment of the primitive chain. In contrast, our results reveal that there is substantial chain stretching that persists well beyond the Rouse time, and it contributes significantly to the initial stress growth. In particular, stress overshoot is found to be primarily due to chain retraction after considerable stretching rather than chain orientation.

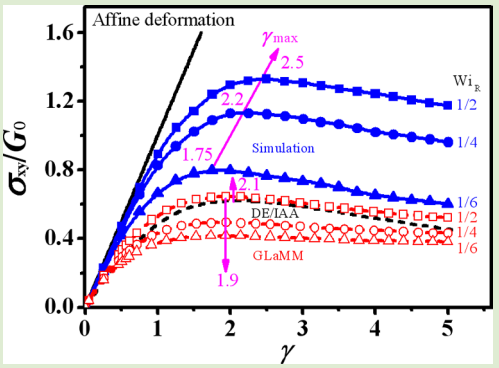

A striking rheological phenomenon in entangled polymer melts[1−5] and solutions[6−11] is stress overshoot during startup shear at sufficiently high rates.[9,10] A widely accepted explanation of this phenomenon[12,13] is based on the tube model.[14] The tube model simplifies the complex, many-body effects of chain interpenetration in terms of a smooth tube-like confinement on a test chain and assumes that the test chain undergoes Rouse dynamics inside the tube. This simplified physical picture leads to decoupling of chain stretching, which is assumed to occur on scales of the Rouse time, τ_R, from chain orientation, which occurs on scales of the reptation time τ_d. Thus, when the shear rate $\dot{\gamma}$ is higher than the reciprocal of the reptation time $1/\tau_d$ but lower than the reciprocal of the Rouse time, $1/\tau_R$, that is, when the Weissenberg number $Wi = \dot{\gamma}\tau_d > 1$ and yet the Rouse-Weissenberg number $Wi_R = \dot{\gamma}\tau_R < 1$, the tube model envisions little stretching of the primitive chain so that the stress is dominated by chain orientation. Consequently, stress overshoot in this regime is attributed to chain alignment in the confining tube by the shear deformation.[13,14]

In spite of its apparent success in describing stress overshoot during startup shear (especially when plotted on log−log scales),[15,16] there has never been direct validation of the molecular mechanism depicted by the tube model.[17] Furthermore, there has been considerable controversy regarding the theoretical implications of a number of particle-tracking velocimetric observations from S.-Q. Wang's group.[18,19] Thus, there is a strong need to use molecular simulation to directly examine the molecular mechanism and test the tube model predictions.

In this Letter, we report results from Brownian dynamics (BD) simulation aimed to explicitly elucidate the molecular origin of stress overshoot upon startup shear of entangled polymer melts under conditions $Wi > 1$ and $Wi_R < 1$. Our results demonstrate that the stress associated with the chain orientation continues to increase with strain well past the maximum of the total shear stress. There is significant chain stretching up to many Rouse times, which contributes substantially to the total stress. In particular, the stress maximum σ_{max} correlates closely with the maximum in chain stretching. Both σ_{max} and the strain at the stress maximum, γ_{max}, increase with shear rates, but results for the different rates are superposable into a master curve when the stress and strain are both scaled by their corresponding σ_{max} and γ_{max}, and this master curve coincides with that obtained from the experimental data.[11]

We use the standard Kremer−Grest model,[20] where monomers are modeled as beads interacting through a truncated and shifted 6−12 Lennard-Jones potential with a cutoff radius $r_c = 2^{1/6}d$, and chain connectivity is modeled by the finitely extensible nonlinear elastic (FENE) potential between adjacent monomers, with a spring constant $k = 30$ in reduced units and fully stretched bond length $R_0 = 1.5d$.[20] This choice of parameters ensures no chain crossing for the shear rates used in our simulation.[21−23] The simulation uses standard Brownian dynamics in the LAMMPS platform. The system consists of 423 chains of length $N = 500$ at a monomer density of $\rho = 0.85d^{-3}$ in a box of volume $V = L_xL_yL_z$, with $L_x = L_y = 6R_{g0}$, and $L_z = 4R_{g0}$, where x, y, and z refer to the flow,

Received: April 30, 2014
Accepted: May 29, 2014
Published: May 30, 2014

gradient, and vorticity directions, and R_{g0} is the equilibrium radius of gyration. Length, energy, and time are non-dimensionalized respectively by the monomer diameter d, energy parameter ε, and the Lennard-Jones time scale $\tau_{LJ} = (md^2/\varepsilon)^{1/2}$, where m is the mass of the particle. The temperature is chosen such that $k_BT = 1$. The simulation time step is $\Delta t = 0.001\tau_{LJ}$. In the quiescent state, the number of monomers in an entanglement strand is found to be $N_e \approx 36$ determined from the crossover time (from $t^{1/2}$ to $t^{1/4}$ scaling) in the monomer mean-square displacement, in agreement with the known literature value.[20,24] The Rouse time τ_R is determined from $\tau_R = (1/3\pi^2)\cdot 6\langle R_{g0}^2\rangle/D_R$,[14] where D_R is the Rouse self-diffusion constant obtained by extrapolation of simulation data of nonentangled polymers. The reptation time τ_d is obtained by the relation $\tau_d/\tau_R = D_R/D_s$, where D_s is the actual self-diffusion constant.[14] Numerically consistent with previous results,[20] we find τ_R and τ_d are 2.3×10^5 and 3.3×10^6, respectively.

We initialize our system by lattice Monte Carlo sampling allowing chain crossing[25] to achieve rapid entanglement of the chains. We then switch to BD and further equilibrate the system for a time τ_d. Conformation properties, such as the mean square internal distances $\langle(\vec{r}_i - \vec{r}_j)^2\rangle/|i - j|$[26] are evaluated to ensure equilibration of the system before turning on shear. The simulation uses periodic boundary condition in the x and z directions and Lees-Edwards boundary condition in the y direction.[27] The data reported are results of averaging over 16 independent samples. Three different shear rates $\dot{\gamma} = (1/6)\tau_R^{-1}$, $\dot{\gamma} = (1/4)\tau_R^{-1}$, and $\dot{\gamma} = (1/2)\tau_R^{-1}$ have been used; below we designate the shear rates using the Rouse-Weissenberg number $Wi_R = \dot{\gamma}\tau_R$.

The shear stress σ_{xy} is calculated using the well-known microscopic expression:[14]

$$\sigma_{xy}^{\text{micro}} = -\frac{1}{V}\sum_{\alpha,i}\langle F_{ix}^{\alpha} r_{iy}^{\alpha}\rangle \tag{1}$$

where F_{ix}^{α} is the x-component of the total force acting on the monomer i of the αth chain located at $\vec{r}_i^{\alpha}$. Figure 1a shows our simulation results for $\sigma_{xy}^{\text{micro}}$ versus strain for the three different shear rates. For comparison, we include results from two versions of the tube theory, the original Doi–Edwards model[14] (hereafter referred to as the DE model or DE) and the more refined GLaMM theory.[15] In the tube model, the shear stress is calculated by using the following expression from the primitive chain[14,15]

$$\sigma_{xy}^{\text{intra}} = \frac{3G_0}{Zl_0^2}\int_0^Z \left\langle \frac{\partial R_x}{\partial s}\frac{\partial R_y}{\partial s}\right\rangle \mathrm{d}s \tag{2}$$

where $G_0 = ck_BT$,[28] with c the number of tube segments per unit volume given by $c = \rho/N_e$, $Z = N/N_e$ is the number of entanglements per chain, l_0 is the Kuhn length for the primitive chain (i.e., the size of a tube segment), and s is the curvilinear coordinate along the primitive chain. The DE model ignores the small amount of chain stretching for $Wi_R < 1$, so that eq 2 can be reduced to

$$\sigma_{xy}^{\text{DE}} \approx 3G_0S_{xy} \tag{3}$$

where S_{xy} is the same-point correlation function for the unit tangent $\vec{u}(s)$ and is given by

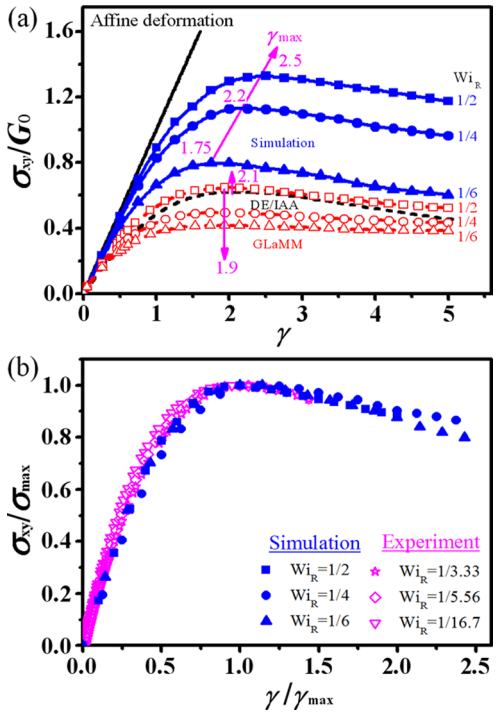

Figure 1. (a) Stress vs strain during startup shear under the condition of $Wi_R < 1$ and $Wi > 1$. For comparison, the stress–strain relations for affine deformation and predicted by the DE theory under the independent alignment approximation (DE/IAA, black dashes) and by the GLaMM theory[30] (red symbols) are included. (b) Master curve for the normalized stress $\sigma_{xy}(\gamma)/\sigma_{max}$ as a function of the normalized strain γ/γ_{max} from (a) and experimental data in ref 11.

$$S_{xy} = Z^{-1}\int_0^Z ds\langle u_x(s)u_y(s)\rangle \tag{4}$$

The GLaMM theory is a refined theory that includes all the key components in the tube model: reptation, chain stretching/retraction, contour length fluctuation, convective constraint release and variable number of entanglements, and is supposed to cover the full range of deformation rate.[15] The GLaMM theory solves for the tangent correlation function tensor $f(s,s') = \langle(\partial\vec{R}(s)/\partial s)(\partial\vec{R}(s')/\partial s')\rangle$. The shear stress is then obtained by taking the xy component of $f(s,s')$ with $s' = s$.[15,29]

For additional comparison, we also include stress produced by an affine deformation that is given straightforwardly as $\sigma_{xy} = G_0\gamma$.

As shown in Figure 1a, both versions of the tube theory considerably under-predict the stress compared with the simulation data. Also, consistent with the experimental observation,[11] the stress overshoot and the peak strain from the simulation increase appreciably with shear rate, but the data for the three shear rates approximately collapse onto a single master curve upon normalizing respectively by σ_{max} and γ_{max} and this master curve agrees with that obtained from the experiment;[11] see Figure 1b. In contrast, the stress predicted by DE is independent of the shear rate. The stress calculated from GLaMM shows modest increase with shear rate, but the location of the stress maximum remains nearly independent of the shear rate, and the overall quantitative discrepancy from the simulation results is actually larger than the DE model. Furthermore, both the DE model and the GLaMM theory yield initial slopes that are less than 1 in the stress–strain curve,

dx.doi.org/10.1021/mz500260h | ACS Macro Lett. 2014, 3, 569–573

in contrast to the simulation data which yield an initial slope of 1 for all shear rates, the slope of the affine deformation.

To understand the origin of the discrepancy between the simulation results and the tube model predictions shown in Figure 1, it is instructive to separately examine the orientational and the remaining contributions in stress. To do so, we compute the stress from the simulation using the intrachain expression, eq 2. However, the use of eq 2 and later the calculation of the contour length require the identification of the primitive chain from the monomer coordinates. Such a method is not provided by the tube model. Primitive chains defined by existing PPA methods[22,31−33] are not suitable for computing the stress using eq 2 since these methods involve deforming the chains from their in situ conformations. We therefore propose the following method for constructing a discrete primitive chain. The chain is divided into $Z = N/N_e$ units with $N_e \approx 36$ monomers in each unit, which serves as a tube segment. The center of mass of the N_e monomers in the unit is $\vec{R}_s$. The stress formula eq 2 can then be discretized into

$$\sigma_{xy}^{\text{intra}} = \frac{3G_0}{(Z-1)l_0^2}\sum_{s=1}^{Z-1}\langle(\vec{R}_{s+1}-\vec{R}_s)_x(\vec{R}_{s+1}-\vec{R}_s)_y\rangle \quad (5)$$

In this construct, N_e serves as a coarse-graining scale for defining the primitive chain, consistent with the intuitive picture of the primitive chain in the tube model. As can be seen in Figure 2, the stress calculated using eq 5 is in good agreement with that calculated from eq 1, confirming the validity of our coarse-graining method.

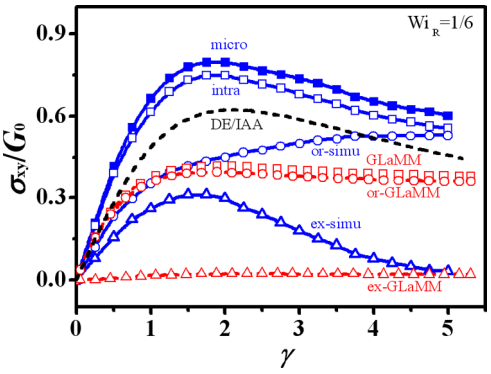

Figure 2. Stress contributions at $Wi_R = 1/6$. The notation "micro" and "intra" designates stress calculated by the microscopic expression eq 1 and intrachain expression eq 5, respectively; "or-simu" and "ex-simu" are, respectively, the orientational and excess stress from the simulation; "or-GLaMM" and "ex-GLaMM" are the corresponding quantities calculated from the GLaMM theory.

We can separately compute the orientational stress using the intrachain expression, eq 5, by converting the bond vector into the unit vector

$$\sigma_{xy}^{\text{or}} = \frac{3G_0}{Z-1}\sum_{s=1}^{Z-1}\left\langle\frac{(\vec{R}_{s+1}-\vec{R}_s)_x(\vec{R}_{s+1}-\vec{R}_s)_y}{(\vec{R}_{s+1}-\vec{R}_s)^2}\right\rangle \quad (6)$$

We define the difference between the full intrachain stress and the orientational stress as the excess stress. In Figure 2 we show the total stress, the orientational stress, and the excess stress from the simulation and from the DE and GLaMM theories, for $Wi_R = 1/6$, which provides a closer test for the $Wi_R < 1$ regime. The DE model has only the orientational stress. The GLaMM theory in principle allows stretching contributions, but the stress is dominated by orientation. Both the DE and GLaMM theories predict stress overshoot arising from the orientational contribution, whereas the orientational stress from the simulation increases monotonically without a peak. The excess stress from simulation contributes significantly to the overall stress up to many Rouse times and exhibits a pronounced peak. Since the orientational stress alone does not produce an overshoot, the overshoot must be due to stretching in the sense that there would be no overshoot in the absence of chain stretching.

The anticipated chain stretching should result in an increase of the contour length of the primitive chain. To obtain the contour length, we calculate the linear distance between two consecutive tube segments from $|\vec{R}_{s+1} - \vec{R}_s|$. The average contour length is then $L = \Sigma_{s=1}^{Z-1}\langle|\vec{R}_{s+1} - \vec{R}_s|\rangle$. The bond length l is obtained from $L = (Z-1)l$, as depicted in the inset of Figure 3; at equilibrium, $l = l_0$, so the equilibrium length is $L_0 = (Z-1)l_0$.[34] The simulation data in Figure 3 show pronounced peaks for all three shear rates, spanning several strain units, corresponding to many Rouse times. In contrast, the GLaMM theory predicts nearly a monotonic approach to steady state with very faint peaks; the peaks are nearly imperceptible for $Wi_R = 1/6$ and $1/4$ on the scales of the figure. The nonmonotonic change of the contour length in the simulation results indicates significant chain stretching followed by retraction. Here, too, the initial increase of the chain contour length follows closely that for affine deformation, which is given simply by $L/L_0 = (1 + \gamma^2/3)^{1/2}$. That the peak in the contour length occurs at roughly the same strain where the shear stress overshoots in Figure 1a points strongly to chain stretching and retraction (which are coupled to orientation) as the root cause of stress overshoots.

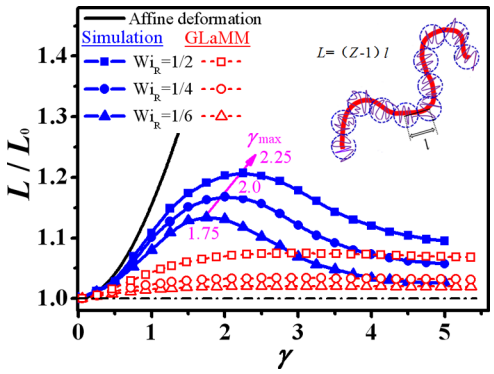

Figure 3. Evolution of the normalized contour length of the primitive chain as a function of strain.

In our recent work,[35] we observed that, under conditions $Wi > 1$ and $Wi_R < 1$, up to many Rouse times, the decline in the number of original entanglements is slower than that under the equilibrium condition and rapid decline of the original entanglements occurs only at sufficiently large strains. Figure 4 shows the evolution of the survival probability of the original entanglements P, which is obtained by normalizing the number of surviving original entanglements for a tagged chain by the equilibrium value of the number of entanglements per chain, both obtained using the PPA method with energy minimization.[22] The crossing time between this probability with the corresponding probability at equilibrium decreases with increasing shear rate. Remarkably, the crossing time for each

dx.doi.org/10.1021/mz500260h | ACS Macro Lett. 2014, 3, 569−573

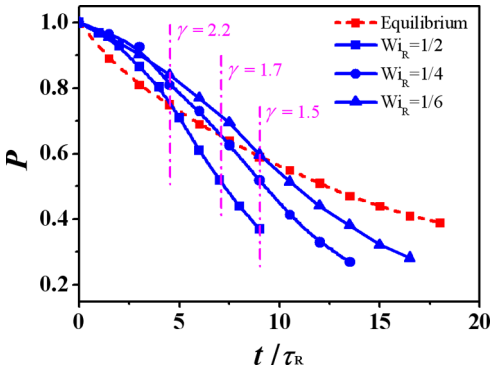

Figure 4. Survival probability of original entanglements as a function of time in units of τ_R.

shear rate in the survival probability corresponds closely to the peak strain of the contour length. This observation suggests that stretching of the chain contour is associated with the initial deformation of a "tightened" network (relative to the equilibrium state), while chain retraction is associated with the loss of the entanglements, when the intrachain retraction force exceeds the interchain forces that hold the network.[36] Since the survival probability of the original entanglements depends on the chain relaxation dynamics, a higher shear rate can produce a greater degree of chain deformation, leading to higher peak strain and peak stress, although the peak time is shorter. That σ_{max} is nearly linearly proportional to γ_{max} (as indicated by the purple arrow in Figure 1a) implies that the stress maxima attained with different shear rates correspond to entanglement networks whose effective elastic moduli have roughly the same value.

In conclusion, using BD simulation, we have examined the molecular origin of stress overshoot in startup shear of entangled polymer melts under conditions of $Wi > 1$ and $Wi_R < 1$. Our results reveal that there is significant change in the primitive chain contour length and that chain stretching contributes substantially to the overall stress. Chain stretching and retraction take place over many Rouse times in this rate regime. For $Wi_R = 1/6$, substantial chain retraction does not occur until $\gamma = 1.75$ corresponding to $10.5\tau_R$. We conclude that retraction of the stretched chains, rather than chain alignment, is the primary cause of stress overshoot. That both chain stretching and shear stress initially follow the affine deformation behavior up to strains of order one (and up to many Rouse times) suggests the active role of interchain forces not captured in the tube construct. While the exact nature of these forces remains to be elucidated by future work, the strong correlation between the contour length and the survival probability of the original entanglements suggests that chain stretching is associated with the deformation of an intact entanglement network, while retraction results from the rapid disentanglement at sufficiently large strains. These findings call into question the barrier-free chain retraction mechanism as envisioned in the tube model, at least for startup shear, and motivate the development of improved or alternative theories.

AUTHOR INFORMATION

Corresponding Authors

*E-mail: ljan@ciac.jl.cn.
*E-mail: swang@uakron.edu.
*E-mail: zgw@caltech.edu.

Notes

The authors declare no competing financial interest.

ACKNOWLEDGMENTS

This work is supported, in part, by the National Natural Science Foundation of China (Nos. 21120102037, 21334007, and 21304097) and further subsidized by the Special Funds for National Basic Research Program of China (No. 2012CB821500).

REFERENCES

(1) Vinogradov, G. V.; Belkin, I. M. *J. Polym. Sci., Part A: Polym. Chem.* **1965**, *3*, 917.
(2) Collis, M. W.; et al. *J. Rheol.* **2005**, *49*, 501.
(3) Auhl, D.; Ramirez, J.; Likhtman, A. E.; Chambon, P.; Fernyhough, C. *J. Rheol.* **2008**, *52*, 801.
(4) Boukany, P. E.; Wang, S.-Q.; Wang, X. R. *J. Rheol.* **2009**, *53*, 617.
(5) Hernadez, A. R.; Detcheverry, F. A.; Peters, B. L.; Chappa, V. C.; Schweizer, K. S.; Muller, M.; de Pablo, J. J. *Macromolecules* **2013**, *46*, 6287.
(6) Huppler, J. D.; MacDonald, I. F.; Ashare, E.; Spriggs, T. W.; Bird, R. B.; Holmes, L. A. *Trans. Soc. Rheol.* **1967**, *11*, 181.
(7) Menezes, E. V.; Graessley, W. W. *J. Polym. Sci., Polym. Phys. Ed.* **1982**, *20*, 1817.
(8) Pearson, D.; Kiss, A. D.; Fetters, L. J.; Doi, M. *J. Rheol.* **1989**, *33*, 517.
(9) Osaki, K.; Inoue, T.; Isomura, T. *J. Polym. Sci., Part B: Polym. Phys.* **2000**, *38*, 1917.
(10) Osaki, K.; Inoue, T.; Isomura, T. *J. Polym. Sci., Part B: Polym. Phys.* **2000**, *38*, 2043.
(11) Ravindranath, S.; Wang, S.-Q. *J. Rheol.* **2008**, *52*, 681.
(12) Snijkers, F.; Vlassopoulos, D. *J. Rheol.* **2011**, *55*, 1167.
(13) Snijkers, F.; Vlassopoulos, D.; Ianniruberto, G.; Marrucci, G.; Lee, H.; Yang, J.; Chang, T. *ACS Macro Lett.* **2013**, *2*, 601.
(14) Doi, M.; Edwards, S. F. *The Theory of Polymer Dynamics*; Clarendon: New York, 1986.
(15) Graham, R. S.; Likhtman, A. E.; McLeish, T. C. B.; Milner, S. T. *J. Rheol.* **2003**, *47*, 1171.
(16) McLeish, T. C. B. *Adv. Phys.* **2002**, *51*, 1379.
(17) Stress overshoot was reported in a recent computer simulation study by Cao and Likhtman, see Cao, J.; Likhtman, A. E. *Phys. Rev. Lett.* **2012**, *108*, 028302. However, their work focused on demonstrating shear banding and did not attempt to explain the molecular mechanism of stress overshoot. Furthermore, the polymer chains were shorter and stiffer than the polymers we use in our work..
(18) Wang, S.-Q.; Ravindranath, S.; Boukany, P. E.; Olechnowicz, M.; Quirk, R. P.; Halasa, A. *Phys. Rev. Lett.* **2006**, *97*, 187801.
(19) Wang, S.-Q.; Wang, Y. Y.; Cheng, S. W.; Li, X.; Zhu, X. Y.; Sun, H. *Macromolecules* **2013**, *46*, 3147.
(20) Kremer, K.; Grest, G. S. *J. Chem. Phys.* **1990**, *92*, 5057.
(21) Kumar, S.; Larson, R. G. *J. Chem. Phys.* **2001**, *114*, 6937.
(22) Sukumaran, S. K.; Grest, G. S.; Kremer, K.; Everaers, R. *J. Polym. Sci., Part B: Polym. Phys.* **2005**, *42*, 917.
(23) Kröger, M.; Loose, W.; Hess, S. *J. Rheol.* **1993**, *37*, 1057.
(24) PPA analysis in ref 22 gives an average number of segments between entanglements $N_{seg} \approx 72 \approx 2N_e$. The factor of 2 arises from different definitions of N_e, which has been discussed in ref 37. Other than setting the modulus G_0, the actual values of N_e are not important (within some reasonable range) and will only affect the numerical accuracy of the discretization in eqs 5 and 6.
(25) Shaffer, J. S. *J. Chem. Phys.* **1994**, *101*, 4205.
(26) Auhl, R.; Everaers, R.; Grest, G. S.; Kremer, K.; Plimpton, S. J. *J. Chem. Phys.* **2003**, *119*, 12718.
(27) Lees, A. W.; Edwards, S. F. *J. Phys. C* **1972**, *5*, 1921.
(28) Note our definition of G_0 differs from G_e in ref 14 by a factor of 1/3, that is, $G_e = 3G_0$.
(29) G_e in ref 15 is related to G_0 by a factor of 4/5, that is, $G_e = 5G_0/4$. The GLaMM theory includes an additional convective contribution

to stress, which is numerically negligible for shear rates considered here.
(30) We chose the parameters in the GLaMM theory[15] to be α_d = 1.15, c_n = 0.1 and $\mathcal{R}_s$ = 2.0 for the contour length fluctuation, constraint release and retraction terms, respectively, and used the number of chain entanglements Z = 14. These parameters are identical to those use in Graham, R. S.; Henry, E. P.; Olmsted, P. D. *Macromolecules* **2013**, *46*, 9849 in their comments on our recent work, ref 35.
(31) Zhou, Q.; Larson, R. G. *Macromolecules* **2005**, *38*, 5761.
(32) Kröger, M. *Comput. Phys. Commun.* **2005**, *168*, 209.
(33) Tzoumanekas, C.; Theodorou, D. N. *Macromolecules* **2006**, *39*, 4592.
(34) We have also computed the contour length by using the radius of gyration r_{ge} of the $N_e \approx 36$ monomers, so that $L/L_0 = r_{ge}/r_{ge0}$; the results are very similar.
(35) Lu, Y. Y.; An, L. J.; Wang, S.-Q.; Wang, Z.-G. *ACS Macro Lett.* **2013**, *2*, 561.
(36) Wang, S.-Q.; Ravindranath, S.; Wang, Y. Y.; Boukany, P. *J. Chem. Phys.* **2007**, *127*, 064903.
(37) Zhou, Q.; Larson, R. G. *Macromolecules* **2006**, *39*, 6737.